Measurement 165 (2020) 108095

Contents lists available at ScienceDirect

Measurement

journal homepage: www.elsevier.com/locate/measurement

Performance enhancements of the spherical detector for pipeline spanning inspection through posture stabilization

Guo Lin, Zeng Zhoumo, Huang Xinjing *, Li Mingze, Feng Hao, Li Jian, Rui Xiaobo

State Key Laboratory of Precision Measuring Technology and Instruments, Tianjin University, Tianjin, China
Binhai International Advanced Structural Integrity Research Centre, Tianjin, China

ARTICLE INFO

Article history:
Received 10 October 2019
Received in revised form 29 May 2020
Accepted 7 June 2020
Available online 27 June 2020

Keywords:
Spanning pipeline
Spherical detector
Rolling stabilization
Acceleration

ABSTRACT

Spherical detector (SD) is promising in the field of subsea pipeline defect detection because of low risk of blockage and quasi-real-time capacity. However, rolling stability has great influence on the detection performance of the SD. This paper proposes posture stabilization measures for enhancing performances of the SD in pipeline spanning inspections via analyzing the mathematical model of detection and experimental validations. Mass of the SD should be concentrated on a plane as much as possible, so that the SD can steadily roll around the unique normal axis with strong immunity to sudden disturbance and uncertainty of launch postures. Especially, when the rotation axis of the SD is one sensitive axis of the triaxial accelerometer equipped, the other two acceleration components can both achieve highest signal to noise ratio and are thus capable of sensitively and reliably detecting low-frequency vibration and downward bend of a spanning steel pipeline.

1. Introduction

Subsea pipeline is the most important way of continuously transporting marine oil and gas resources to land. As offshore oil and gas resources are being vibrantly exploited, the number of subsea pipelines is increasing at an amazing rate. These subsea pipelines are exposed to harsh marine environment for a long time, and have been bearing complex severe working and environmental loads. The fracture risk of these pipelines is very high [1–3]. Once the submarine pipeline breaks, the leaked oil will spread rapidly. The rupture of submarine pipeline will lead to serious and extensive environmental pollution and even ecological disaster. Regular inspection of subsea pipeline, timely detection of defects and potential safety hazards, and appropriate repair measures can avoid the occurrence of subsea pipeline rupture.

Spanning may occur throughout the whole service life of a subsea pipeline, leaving the pipeline frequently in a dangerous situation [4–6]. Spanning can occur when the pipeline is laid onto uneven sea bottom, or during long period of service due to the erosion by the ocean current. Spanning pipeline is prone to bend down causing stress concentration. In addition, when the ocean current bypasses the spanning pipeline, alternating vortexes will be induced behind the pipeline and drag the pipe to vertically vibrate [7,8], which is well known as vortex-induced vibration. Severe bend and vibration will cause overload axial stresses to a spanning pipe and lead to fracture. In order to prevent pipeline spanning from deterioration and fracture through timely reinforcement, monitoring or quasi-real-time detection of subsea pipeline spanning must be carried out.

Underwater robots such as ROVs (Remotely Operated Vehicles) and AUVs (Autonomous Underwater Vehicles) [9,10], can be used for observing and looking for pipeline spanning via acoustic or optical imaging. However, as deployment of ROV and AUV is very costly and long-periodic, underwater robots cannot realize monitoring or quasi-real-time detection of subsea pipeline spanning. Distributed optic fiber was proposed to monitor subsea pipeline spanning via sensing dynamic strain of a vibrating spanning pipe, static strain of a bent spanning pipe, or temperature drop because of ocean current scour [11–13]. However, there are few subsea pipelines with optic fibers, as it is extremely difficult to lay fiber along with the pipeline [14].

In-pipe detectors, as the main means of ashore pipeline inspection, may be competent for quasi-real-time detection of subsea pipeline spanning with the advantages of not being constrained by external environment, high efficiency and high accuracy. There are two kinds of in-pipe detectors: cylindrical Pipeline Inspection Gauges, PIGs and Spherical Detectors, SDs. PIGs [15,16] are widely used in land pipelines. PIGs are very difficult to be applied in subsea pipelines because of its large volume, close contact with the

* Corresponding author.
E-mail address: huangxinjing@tju.edu.cn (H. Xinjing).

https://doi.org/10.1016/j.measurement.2020.108095
0263-2241/

pipe wall, and being easy to cause blockage. SDs [17,18] have the advantages of being easy to use but not being easy to block, and the passability of the SD has been experimentally verified [19]. Recently, the latest promising uses of the SD and its advantages of quasireal-time detection have been demonstrated via subsea pipeline 3D localization [20], inflection point detection, and magnetic anomaly detection [21], and pipeline inclination measurement [22].

In 2019, the authors of this paper [23] proposed a method of using the SD to detect subsea spanning pipeline vibration, and analytically and experimentally demonstrates how to extract the vibration frequency of a spanning pipeline from the acceleration signal recorded by the SD. This method can work very well, if the SD rotates around a fixed axis, or if the acceleration signals due to vibration is very noticeable when the spanning pipeline severely vibrates or the vibration frequency is not too low. However, the rotation axis is not absolutely fixed; it may sway. When the pipeline span becomes longer as scour develops, the vibration frequency will go lower, and the weak vibration acceleration will be submerged in rolling-caused signals and noises and is thus difficult to extract.

This paper will analyze the output mathematical model of the accelerometer in the SD while rolling forward, and provide the structural optimization idea aiming for stabilizing the SD rolling posture and enhance pipeline spanning detection performances. Through smart design of the SD structure and comprehensive experimental validation, the conditions of achieving a stable, knowable and anti-interference axis-fixed rotation is obtained. Both rolling noise reduction and vibration sensitization of the accelerometer are realized.

2. Detection principle and optimization motivation

The working principle of the SD for detecting subsea pipeline spanning is shown in Fig. 1(a). The SD carries a triaxial accelerometer and rolls forward under the impetus of the fluid in the pipeline. When the SD passes through a spanning pipeline, pipeline bend or vortex-induced vibration will cause abnormal changes in the acceleration signals recorded by the SD. After inspection is finished, the spanning pipeline is identified via analyzing the recorded acceleration signals off line. Previous field experiments have demonstrated that the SD can basically rotate around a fixed axis [20,21] which may point at an arbitrary direction. When the pipeline is flat and straight, the rotation angular speed of the SD is constant.

As shown in Fig. 1(b), the pipe coordinate system is defined and denoted as O_1-$X_1Y_1Z_1$, the sensor coordinate system is O_2-$X_2Y_2Z_2$, and the SD coordinate system is O_3-$X_3Y_3Z_3$. The origin of the frame O_1-$X_1Y_1Z_1$ is located at the sphere center, and moves together with the SD, but does not rotate together with the SD. The origin of the frame O_3-$X_3Y_3Z_3$ is also located at the center of the sphere; It moves and rotates together with the SD. The axis $\mathbf{Y}_3$ is parallel to $\mathbf{Y}_1$. Assuming that the angular frequency of the rotation of the SD is $\omega_1 = 2\pi f_1$, the transformation matrix from the frame O_3-$X_3Y_3Z_3$ to O_1-$X_1Y_1Z_1$ is as follows:

$$\mathbf{R}_{13} = \begin{bmatrix} \cos\omega_1 t & 0 & \sin\omega_1 t \\ 0 & 1 & 0 \\ -\sin\omega_1 t & 0 & \cos\omega_1 t \end{bmatrix} \tag{1}$$

The position and posture of the accelerometer in the frame O_3-$X_3Y_3Z_3$ are fixed once the SD assembly is completed. Therefore, the transformation matrix $\mathbf{R}_{32}$ from the frame O_3-$X_3Y_3Z_3$ to O_2-$X_2Y_2Z_2$ is a constant and satisfies $\mathbf{R}_{32}\mathbf{R}_{32}^T = \mathbf{I}$. Vector $\mathbf{b}=(x_{22}, y_{22}, z_{22})$ is the expression of the rotation axis Y_3 in the sensor frame O_2-$X_2Y_2Z_2$, and $|\mathbf{b}|=1$.

$$\mathbf{R}_{32} = \begin{bmatrix} x_{21} & y_{21} & z_{21} \\ x_{22} & y_{22} & z_{22} \\ x_{23} & y_{23} & z_{23} \end{bmatrix} \tag{2}$$

The transformation matrix from the frame O_2-$X_2Y_2Z_2$ to O_1-$X_1Y_1Z_1$ is formulated as follows:

$$\mathbf{R}_{12} = \mathbf{R}_{13}\mathbf{R}_{32} = \begin{bmatrix} \sqrt{1-x_{22}^2}\cos(\omega_1 t + \varphi_x + \frac{3\pi}{2}) & \sqrt{1-y_{22}^2}\cos\left(\omega_1 t + \varphi_y + \frac{3\pi}{2}\right) & \sqrt{1-z_{22}^2}\cos(\omega_1 t + \varphi_z + \frac{3\pi}{2}) \\ x_{22} & y_{22} & z_{22} \\ \sqrt{1-x_{22}^2}\cos(\omega_1 t + \varphi_x) & \sqrt{1-y_{22}^2}\cos\left(\omega_1 t + \varphi_y\right) & \sqrt{1-z_{22}^2}\cos(\omega_1 t + \varphi_z) \end{bmatrix}, \tag{3}$$

where

$$\cos\varphi_x = x_{23}/\sqrt{1-x_{22}^2},\ \cos\varphi_y = y_{23}/\sqrt{1-y_{22}^2},\ \text{and}\ \cos\varphi_z = z_{23}/\sqrt{1-z_{22}^2}. \tag{4}$$

The output of the accelerometer, $\mathbf{a}=(a_x, a_y, a_z)^T$, is:

$$\begin{aligned} \mathbf{a} &= \mathbf{R}_{21}(0,0,-g)^T + \mathbf{R}_{23}(0,0,\omega_1^2 r_0)^T + \sigma^T \\ &= \mathbf{R}_{12}^T(0,0,-g)^T + \mathbf{R}_{32}^T(0,0,\omega_1^2 r)^T + \sigma^T \end{aligned} \tag{5}$$

where g is the gravitational acceleration constant, and $\boldsymbol{\sigma}$ is the random noise generated by the SD's bumping up and down and the slight vibration of the rotation axis.

For a spanning and vibrating pipeline with a vibration amplitude of A and an angular frequency of $\omega_2 = 2\pi f_2$, it is equivalent to adding an AC component with an acceleration amplitude of $\omega_2^2 A$ to the gravity acceleration constant g. When the SD rolls in such a vibrating pipeline, the output of the accelerometer is:

$$\mathbf{a} = \mathbf{R}_{12}^T(0,0,-g+\omega_2^2 A\cos(\omega_2 t + \varphi'))^T + \mathbf{R}_{32}^T(0,0,\omega_1^2 r_0)^T + \sigma^T \tag{6}$$

where

$$\begin{aligned} a_x = &-g\sqrt{1-x_{22}^2}\cos(\omega_1 t + \varphi_x) \\ &+\frac{1}{2}\omega_2^2 A\sqrt{1-x_{22}^2}[\cos(\omega_2 t + \omega_1 t + \varphi' + \varphi_x) \\ &+\cos(\omega_2 t - \omega_1 t + \varphi' - \varphi_x)] + x_{23}\omega_1^2 r_0 + \sigma_x, \end{aligned} \tag{7}$$

$$\begin{aligned} a_y = &-g\sqrt{1-y_{22}^2}\cos\left(\omega_1 t + \varphi_y\right) \\ &+\frac{1}{2}\omega_2^2 A\sqrt{1-y_{22}^2}\left[\cos\left(\omega_2 t + \omega_1 t + \varphi' + \varphi_y\right)\right. \\ &\left.+\cos\left(\omega_2 t - \omega_1 t + \varphi' - \varphi_y\right)\right] + y_{23}\omega_1^2 r_0 + \sigma_y, \end{aligned} \tag{8}$$

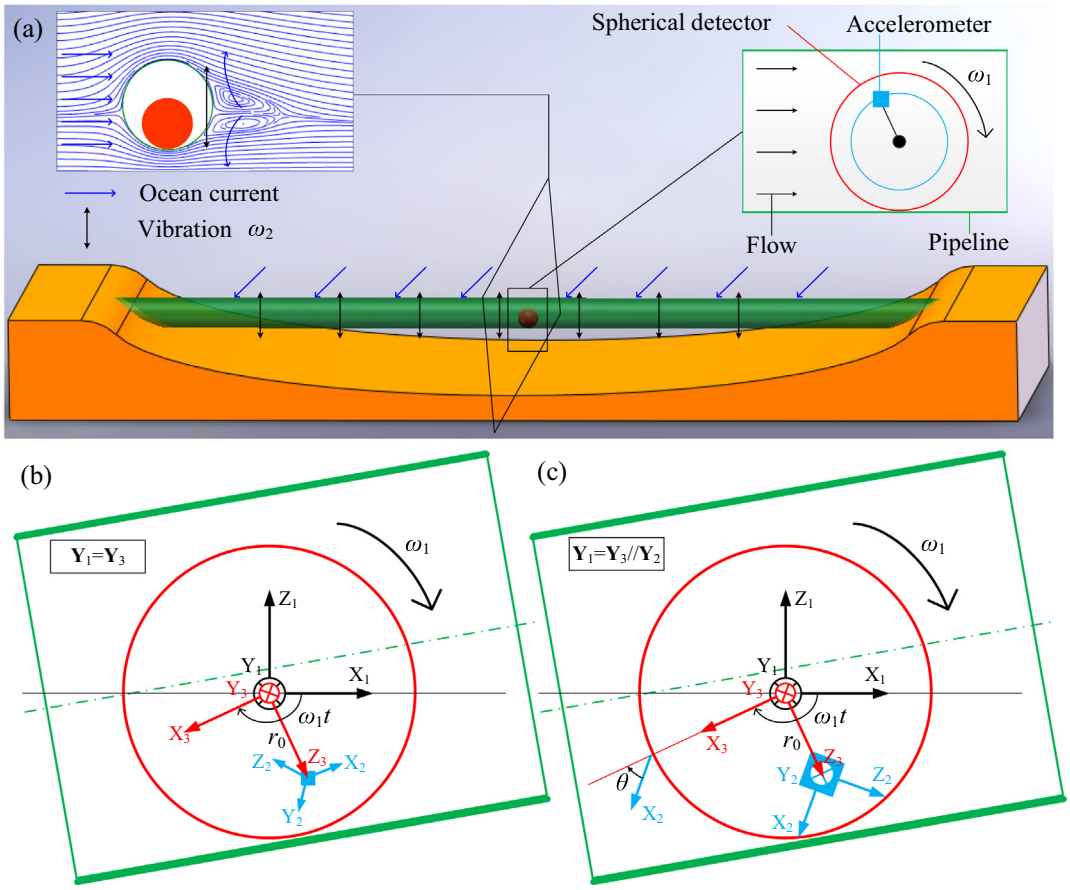

Fig. 1. Schematic of pipeline spanning detection by the SD: The SD is rolling forward inside a vibrating spanning pipeline (a); Frame definitions when the rotation axis points at an arbitrary direction (b), and when the rotation axis is parallel to one sensitive axis of the accelerometer (c).

$$a_z = -g\sqrt{1-z_{22}^2}\cos(\omega_1 t+\varphi_z) + \frac{1}{2}\omega_2^2 A\sqrt{1-z_{22}^2}\left[\cos(\omega_2 t+\omega_1 t+\varphi'+\varphi_z) + \cos(\omega_2 t-\omega_1 t+\varphi'-\varphi_z)\right] + z_{23}\omega_1^2 r_0+\sigma_z. \quad (9)$$

It can be seen from Eqs. (7)–(9) that each component of the vectored acceleration has the same form with regards to the AC component, DC component and noise. The AC component consists of three subcomponents with frequencies of ω_1, $\omega_1-\omega_2$, $\omega_1+\omega_2$, where $\omega_1 = 2\pi f_1$ is rotation frequency of the SD and $\omega_2 = 2\pi f_2$ is pipeline vibration frequency. The DC component is the centripetal acceleration of the accelerometer and is proportional to the square of the rotation frequency. If the rotation axis is not well-designed, effective information related to pipeline vibration will be dispersedly contained in all the three acceleration components, which will weaken the signal to noise ratio. Because the amplitudes of the subcomponents of $\omega_1-\omega_2$ and $\omega_1+\omega_2$, which can indicate pipeline vibration, are $\frac{1}{2}\omega_2^2 A\sqrt{1-p_{22}^2}$ where $p = x, y, z$, the detection sensitivity of pipeline vibration decreases with the decrease of the vibration frequency, and also varies with the change of the rotating axis $\mathbf{b}=(x_{22}, y_{22}, z_{22})$. Therefore, $\mathbf{b}$ must be controlled as much as possible into a constant. If we can further control $\mathbf{b}$ to be parallel to one sensitive axis of the accelerometer, namely, one of $\{x_{22}, y_{22}, z_{22}\}$ is zero, then two of $\frac{1}{2}\omega_2^2 A\sqrt{1-p_{22}^2}$ where $p = x, y, z$ will become $\frac{1}{2}\omega_2^2 A$, the vibration detection sensitivity can be enhanced and is independent of the slight shaking of the rotation axis.

When the rotation axis of the SD is parallel to one of the three sensitive axes of the accelerometer, for example, $\mathbf{b} = \mathbf{Y}_2=(0, 1, 0)$, as shown in Fig. 1 (c), the transformation matrix from the frame O_2-$X_2Y_2Z_2$ to O_3-$X_3Y_3Z_3$ is as follows:

$$\mathbf{R}_{32} = \begin{bmatrix} x_{21} & y_{21} & z_{21} \\ x_{22} & y_{22} & z_{22} \\ x_{23} & y_{23} & z_{23} \end{bmatrix} = \begin{bmatrix} \cos\theta & 0 & -\sin\theta \\ 0 & 1 & 0 \\ \sin\theta & 0 & \cos\theta \end{bmatrix} \quad (10)$$

where θ is the angle by which $\mathbf{X}_2$ rotates around $\mathbf{Y}_3$ to overlap $\mathbf{X}_3$. Substitute the elements of $\mathbf{R}_{32}$ in Eqs. (7)–(9) with the values in Eq. (10), the three-axis outputs of the accelerometer can be rewritten as:

$$a_x = -g\cos(\omega_1 t+\varphi_x) + \frac{1}{2}\omega_2^2 A\left[\cos(\omega_2 t+\omega_1 t+\varphi'+\varphi_x) + \cos(\omega_2 t-\omega_1 t+\varphi'-\varphi_x)\right] + \sin\theta\,\omega_1^2 r_0+\sigma_x \quad (11)$$

$$a_y = \sigma_y \quad (12)$$

$$a_z = -g\cos(\omega_1 t+\varphi_z) + \frac{1}{2}\omega_2^2 A\left[\cos(\omega_2 t+\omega_1 t+\varphi'+\varphi_z) + \cos(\omega_2 t-\omega_1 t+\varphi'-\varphi_z)\right] + \cos\theta\,\omega_1^2 r_0+\sigma_z \quad (13)$$

Eqs. (11)–(13) indicate that if one of the sensitive axes of the accelerometer is parallel to the rotation axis of SD, theoretically there will be no AC component along the rotation axis related to SD rolling; Instead, the AC information will be completely transferred to the other two sensitive axes. On one hand, the effective signal is enhanced; On the other hand, the acceleration component along the rotation axis will only sense the noise that has no statistical characteristics, and therefore can be used to detect abnormal state of the SD during rolling process. In addition, when the spanning pipeline bends downward, the SD rolls downhill and uphill successively with a process of acceleration first and then slowing down, which can be indicated by the fluctuation of the rotation frequency ω_2. However, the premise for this phenomenon to occur is that the SD is capable of steadily rolling around one fixed axis.

There are two key points with respect to maintaining fixed-axis rolling: (1) The rotation axis is unique and self-stable; Even if the launch attitude is different or the rotation axis suddenly varies due to turbulence, the SD can still quickly recover to the desired rotation axis. (2) The rotation axis of the SD is designable and is knowable after the SD design is finished, so that one of the sensitive axes of the accelerometer can be deployed along the rotation axis.

Previous experiments have indicated that the rotation axis may be the axis around which the moment of inertia is the largest among the three. Considering the axial symmetry of the SD, the moment of inertia of the SD can be adjusted by using a heavy cylinder. Because the shell of the SD is much lighter than counterweight cylinder, the moment of inertia of the SD is mainly determined by the internal counterweight cylinder. For a cylinder with radius r, mass m, and height h, as shown in Fig. 2, its moment of inertia is:

$$I_x = I_y = \frac{1}{12}m\left(3r^2 + h^2\right) \text{ and } I_z = \frac{mr^2}{2}, \tag{14}$$

and the ratio of the two is:

$$\frac{I_z}{I_x} = 6/\left(3 + \frac{h^2}{r^2}\right) : \begin{cases} = 2, & if\ h \ll r \\ \le 0.5, & if\ h \ge 3r \end{cases} \tag{15}$$

If $h \ll r$, the counterweight is of disk shape, there is only one axis with larger moment of inertia, i.e. the cylinder axis. If $h \gg r$, the counterweight is of thin rod shape, and there are two axes with larger moments of inertia, i.e. the two cylinder radial directions. For other cases, there is no significant difference among the three moments of inertia. In order to make the rotation axis unique and stable, counterweight of disk shape should be used to maximize I_z and make the disc axis be the rotation axis of the SD. In this case, the rotation axis of the SD is not easy to be changed by external disturbances; Even if rotation axis deflection occurs, the rotation axis of the SD can be redirected to the disk axis in a very short time.

Based on the analysis above and previous tests of the SD, it can be inferred that two main factors can affect the rolling stability of the SD: weight and mass distribution. Proper weight can ensure not only that the SD can always keep in tight touch to the pipeline bottom without noticeable bounce while rolling, but also that the SD can roll around a basically fixed axis. With smart mass distribution, the SD can roll much more stably and can even rotate around a predetermined axis. The rest of this paper will experimentally verify these optimization ideas and performance enhancements of pipeline spanning detection because of structural optimization.

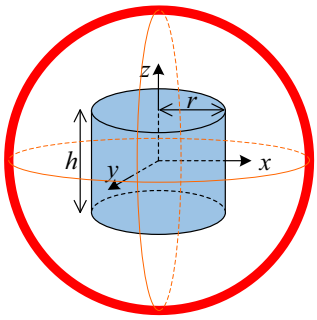

Fig. 2. A cylindrical counterweight inside the SD.

3. Experiments

SDs with different weights and mass distributions were designed and manufactured. In order to analyze the rolling state of the SD, a triaxial accelerometer was mounted in each SD. The acceleration signal recorded was used to study the influence of various factors on the rolling stability. Experiments for comparing pipeline vibration and bend detection performances of the SDs that can or cannot stably roll were also carried out in the end. Experimental apparatus is shown in Fig. 3. A steel pipe with a length of 12 m, an inner diameter of 105 mm, and a wall thickness of 4 mm, was employed for experiments. An air pump was used to inject airflow into the pipe to push the SD to roll forward. A three-way ball valve was used to bypass the flow to control the flow rate, thereby adjusting the thrust to the SD and the rolling speed of the SD. In each test, the SD enters the steel pipe from one end and rolls out from the other end. As at the moment of launching the SD, the airflow velocity at the inlet of the pipe is unstable due to the process of speeding up, a 2 m long PVC pipe is connected to the upstream of the steel pipe as a buffer pipe to stabilize the airflow. There is an additional perturbation in the middle of the pipeline where the SD slightly jumps. This is used to test the SD's recover capacity after it deviates from the initial rotation axis.

In order to test the effects of the weight of the SD on its anti-interference ability, a plastic spherical shell and a Φ35mm plastic hollow cylinder, a Φ16mm steel rod, and a Φ24mm steel rod, as shown in Fig. 4, were used to form three SDs with different weights, numbered as SD-A, SD-B, SD-C, respectively. During this test, the pipeline was laid flat on the ground. The rotation stability of the SD with different weights was evaluated by analyzing the AC and DC component fluctuations of the recorded acceleration signals.

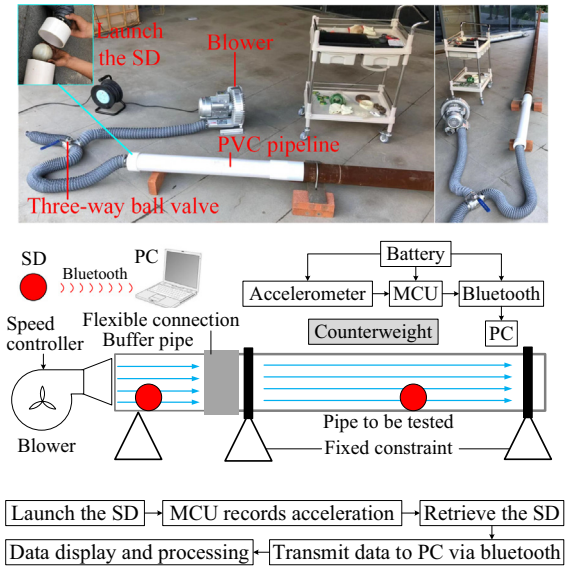

Fig. 3. Experiment apparatus, device composition, and process schematic.

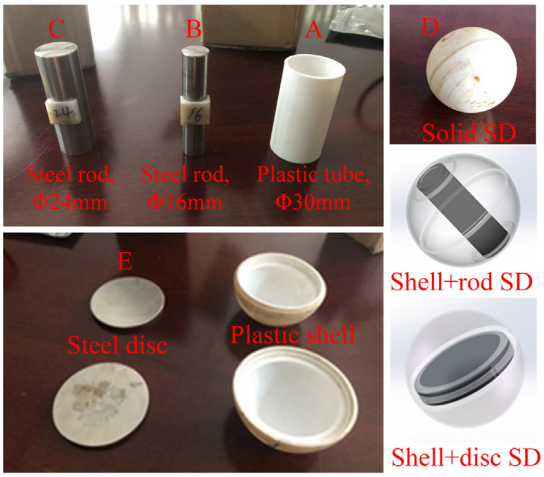

Fig. 4. SDs with different counterweights and sizes.

Three SDs with different mass distributions were employed to demonstrate that mass distribution can determine the rotation axis of the SD and affect the axis-fixed rolling stability as well as restoration capacity after being disturbed. The three SDs have the same spherical plastic shells with the same outer diameter. Mass centroids of them are all in the sphere center, but their moments of inertia around three axes are quite different, since the shape and weight of the counterweights inside are different. These counterweights are steel rod, solid plastic ball, and a steel disc, to form the three SDs numbered as SD-C, SD-D, SD-E, as shown in Fig. 4. The SD-C with a steel rod simulates the situation that the components and parts are concentratedly arranged on one axis. The SD-D with solid structure simulates the situation that the components and parts are uniformly distributed in the whole spherical cavity. The SD-E with a steel disc simulates the situation that the components and parts are concentratedly arranged on one plane. The fixed-axis rotation capabilities of these three SDs were tested and evaluated by analyzing the recorded acceleration signals. Especially, the SD-E with a steel disc was tested for extra many times with different launching angles to demonstrate its axis-fixed rotation capacity.

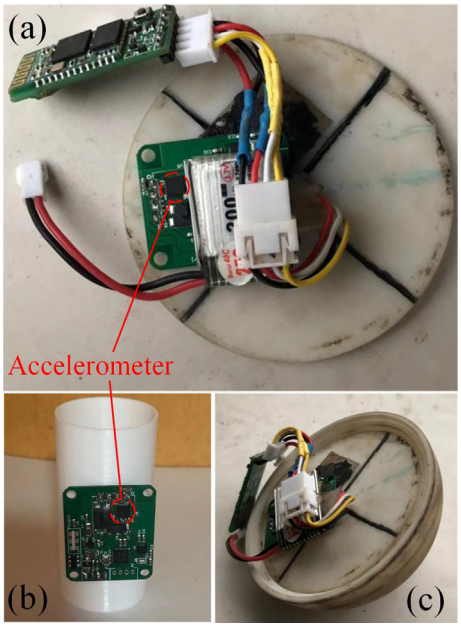

Fig. 5. Installation of accelerometer for experiment.

The installation of the accelerometer in different SDs are shown in Fig. 5. The sampling rate, measurement range, and resolution of the tri-axial accelerometer is 200 Sps, ±16 g, and 0.5 mg, respectively. Because both the rolling frequency of the SD and spanning vibration frequency are no more than 10 Hz, the sampling rate of 200 Sps is fast enough. In the current experiment of this manuscript, the data is transmitted to a personal computer via Bluetooth in real time. In the field application, the data is recorded into a TF card by the micro-controller inside the SD; when the inspection of a pipeline is finished, the SD is taken out of the pipeline, and the data is downloaded in to the personal computer.

Uncertainty analyses of the stability assessment of the SD with various parameters of weight and mass distribution were carried out. These uncertainty analyses used the data in Figs. 6–11. Figs. 6–8 show the data of three times of rolling tests with the SDs with different weights, and their statistical results are shown in Table 1; while Figs. 9–11 show the data of three times of rolling tests with the SDs with different mass distributions, and their statistical results are shown in Table 2.

Seven seconds of acceleration data a_y in Fig. 6/7/8 are divided into three segments: 1–2 s, 3–5 s and 6–7 s, for uncertainty analyses, and the results are listed in Table 1. Amplitude variances of each segment are used to assess the SD's rolling stability. Table 1 lists average amplitudes of each segment, their variances, and three variances' variances, when testing SDs with three similar structures but different weights, SD-A, SD-B, and SD-C. The smaller the variance is, the more stable the rolling state of the SD is. It can be seen from Table 1 that the stability order is SD-C > SD-B > SD-A; namely, the larger the weight is, the more stable the rolling state of the SD is.

Similarly, twenty seconds of acceleration data a_x in Fig. 9/10/11 are divided into four segments: 1–5 s, 6–10 s, 11–15 s, and 16–20 s, for uncertainty analyses, and the results are listed in Table 2 including average amplitudes of each segment, their variances, and three variances' variances, when testing SDs with different mass distributions, SD-C, SD-D, and SD-E. It can be seen from Table 1 that the stability order is SD-E $\gg$ SD-D > SD-C with the variances in ascending order; namely, the SD with the mass concentrated in the middle disc has a most stable rolling state. The

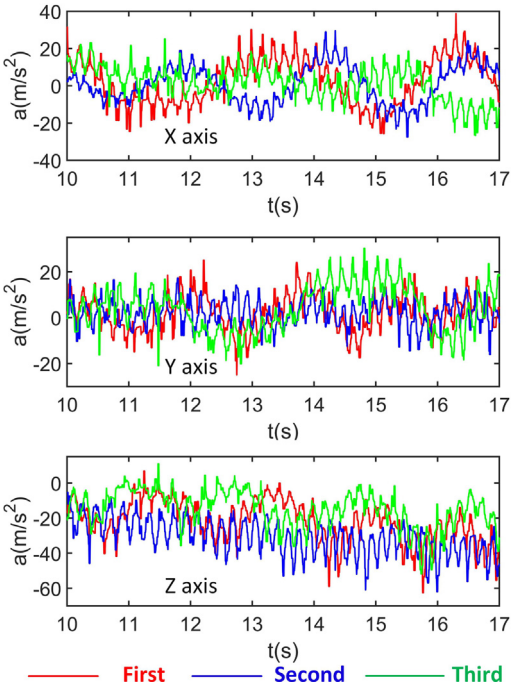

Fig. 6. Acceleration recorded by the lightest SD-A.

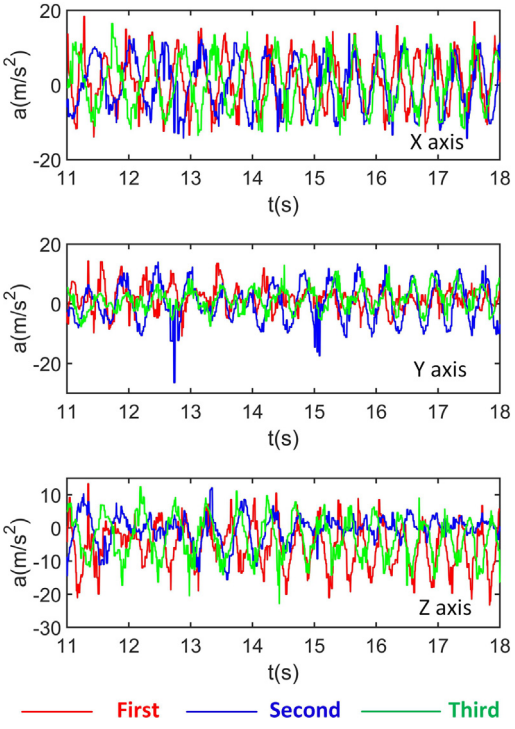

Fig. 7. Acceleration recorded by the SD-B with medium weight.

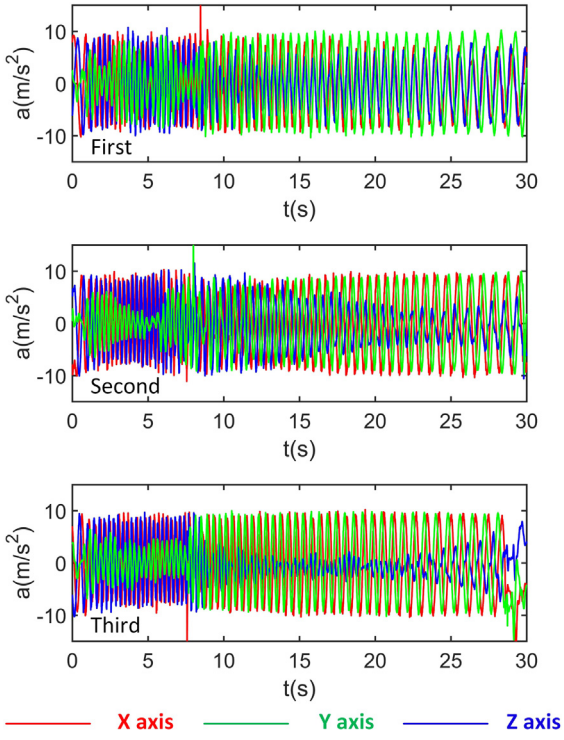

Fig. 9. Acceleration recorded by the solid SD.

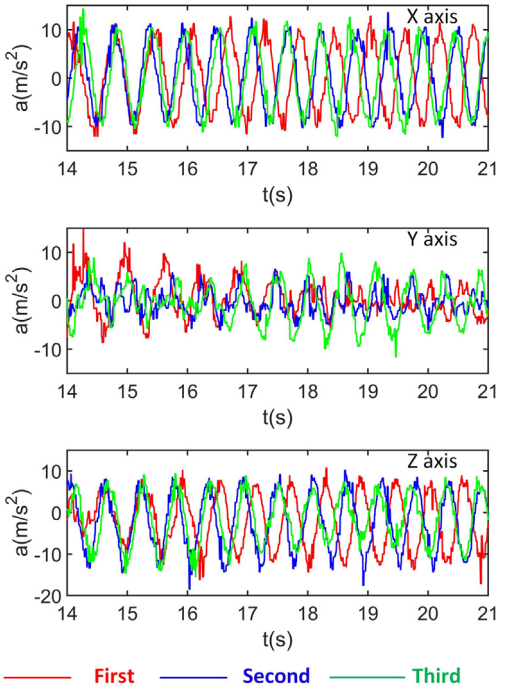

Fig. 8. Acceleration recorded by the heaviest SD-C.

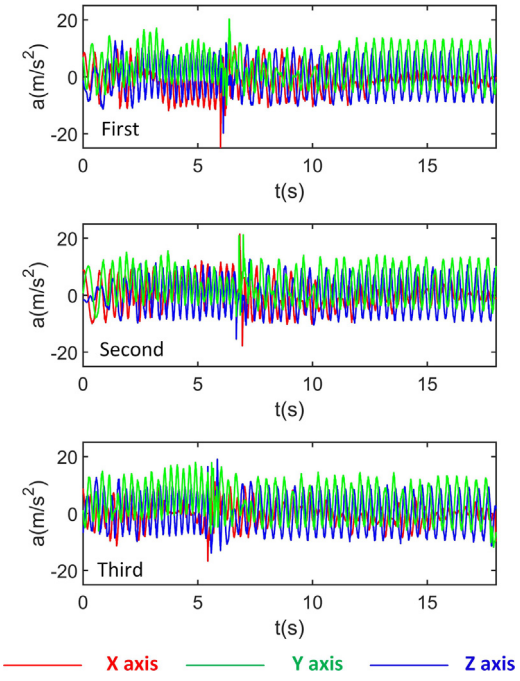

Fig. 10. Acceleration recorded by the SD with a Φ24mm steel rod inside.

amplitude variance of the SD-E is very small, so the SD-E can be approximately considered to be fixed-axis rolling in the pipeline.

4. Results and discussions

4.1. Effects of weight

Three SDs were tested in the pipeline that is laid flat and straight on the ground: the SD-A contains a hollow plastic cylinder, which is the lightest; SD-B contains a Φ16mm steel rod, which has a medium weight; SD-C contains a Φ24mm steel rod, which is the heaviest. These SDs have the same outside diameter. Test experiment for each weight of SD was repeated three times, and the results are shown in Figs. 6–8. With the increase of weight, the fluctuation of AC and DC components of each acceleration component becomes weaker and weaker, indicating that heavier SD rolls more stably. If the SD is not heavy enough, it cannot keep in

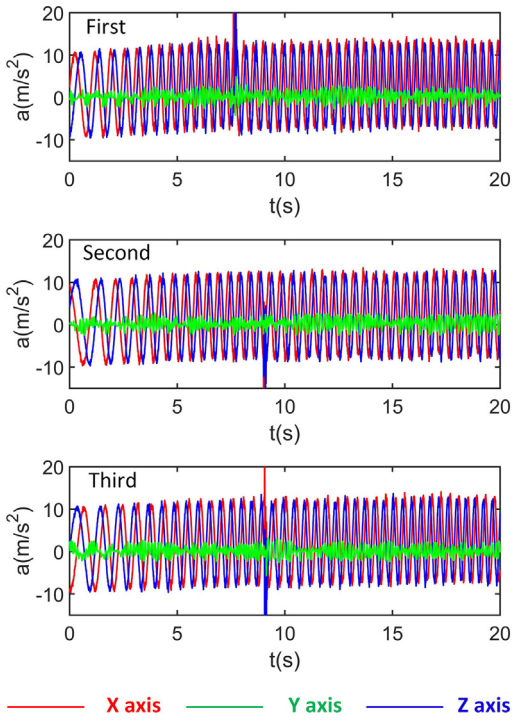

Fig. 11. Acceleration recorded by the SD with a steel disc inside.

continuous contact with the pipe wall and its rolling is easily disturbed by the turbulent flow. For a lighter SD, both the acceleration amplitude and equilibrium point significantly fluctuate, indicating that the rotating axis is always changing while the SD is rolling. Unstable rolling results in frequent hard contact with the pipe wall and a lot of sharp noise in the acceleration signals. Therefore, heavier SD can basically achieve fixed-axis rotation and suppress the noises.

4.2. Influence of mass distribution

The testing results are shown in Figs. 9–11 for the SD-C with a steel rod, the homogeneous solid SD-D, and the SD-E with a steel disc. For the solid SD-D, since there is no significant difference among the three moments of inertia, its rotation axis is always changing, leading to continuous fluctuations of the amplitudes of recorded acceleration, as indicated by the blue Z component in Fig. 9. The SD-C with a steel rod has two axes around which the moments of inertia are close to each other and are both larger than the third one. Therefore, its rotation axis is neither unique nor fixed. The rotation axis of the SD-C can maintain unchanged over a short time but may still suddenly change, as indicated by the red X component in Fig. 10 whose amplitude suddenly changes and then remains unchanged. Therefore, neither of the SD-C and the SD-D have unique rotation axis and can achieve axis-fixed rotation. The SD-E with a steel disc is capable of stably rolling both before and after being disturbed, and its Y component acceleration is always very small, which is consistent with the Eqs. (11)–(13) and (15). When the SD-E is disturbed, its rolling state does not change too much and it can quickly recover to the previous stable rolling state. Three test results of the SD-E have high similarity with each other, which proves that the structure-optimized SD can stably rotate around a unique and fixed axis.

The SD-E with a steel disc inside is the most stable among all the five tested SDs; its rotation axis is difficult to change so it has excellent capacity of anti-disturbance and self-stabilizing. The uniqueness of its rotating axis was further verified via launching the ball with different initial postures, as shown in Fig. 12. The angle between the pipe axis and the plane where the disc is located is denoted as α. The speeding up process of the SD-E after being launched was recorded respectively with the initial states of $\alpha = 0^{\circ}$, $\alpha = 30^{\circ}$, $\alpha = 45^{\circ}$, $\alpha = 60^{\circ}$ and $\alpha = 90^{\circ}$. As shown in Fig. 13, for different α, even though the initial rotation axes are different from the disc axis, the SD-E can eventually turn to rotate around the disc axis with the largest moment of inertia. This demonstrates that the rotation axis of the SD-E containing a steel disc is unique,

Table 1
Stability comparison of SDs with different weights.

Type of SD	Number of experiments	Average amplitude in 1–2 s (m/s^2)	Average amplitude in 3–5 s (m/s^2)	Average amplitude in 6–7 s (m/s^2)	Variance of average amplitude	Average of variance
SD-A	1st	12.67	7.13	7.56	2.52	2.06
	2nd	6.14	9.58	7.06	1.45	
	3rd	11.53	6.48	10.64	2.20	
SD-B	1st	10.39	7.72	6.19	1.74	1.78
	2nd	8.85	9.06	12.44	1.65	
	3rd	5.17	8.34	9.87	1.96	
SD-C	1st	8.13	4.67	3.98	1.82	1.06
	2nd	3.96	4.45	4.32	0.21	
	3rd	5.56	8.41	6.79	1.17	

Table 2
Stability comparison of SDs with different mass distributions.

Type of SD	Number of experiments	Average amplitude in 1–5 s (m/s^2)	Average amplitude in 6–10 s (m/s^2)	Average amplitude in 11–15 s (m/s^2)	Average amplitude in 16–20 s (m/s^2)	Variance of average amplitude	Average of variance
SD-D	1st	9.19	8.97	8.53	7.87	0.45	0.56
	2nd	9.32	9.66	7.21	8.85	1.02	
	3rd	9.14	9.31	9.76	9.79	0.22	
SD-C	1st	7.74	7.22	4.37	2.61	1.90	1.48
	2nd	7.66	7.43	5.11	3.89	1.47	
	3rd	5.92	5.44	4.27	2.83	1.07	
SD-E	1st	9.93	10.01	9.98	9.89	0.05	0.05
	2nd	10.06	10.12	9.99	9.97	0.07	
	3rd	9.96	10.03	9.97	10.01	0.02	

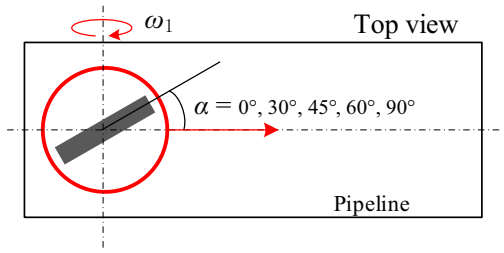

Fig. 12. The SD-E with a steel disc inside is launched with different initial postures.

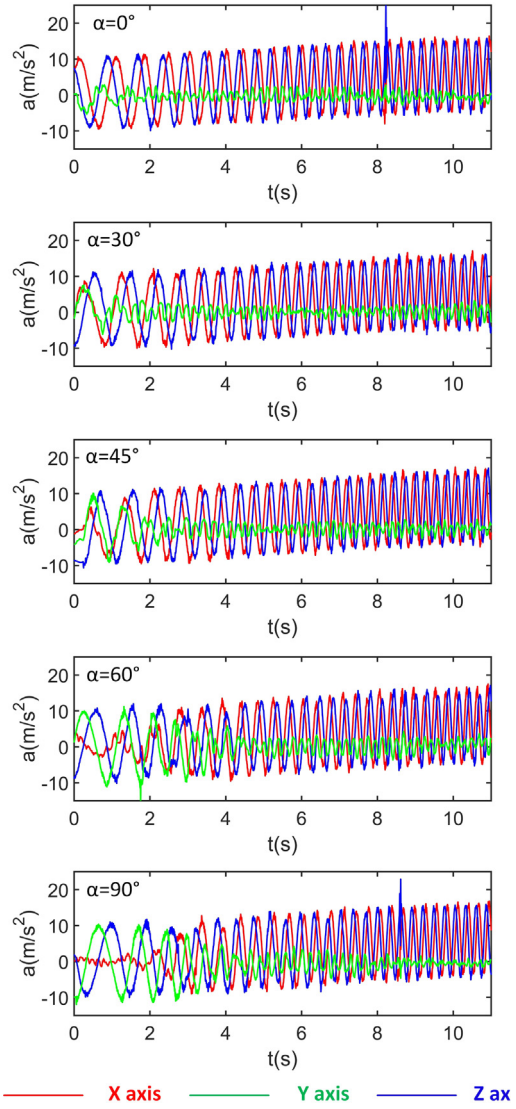

Fig. 13. Uniqueness of the rotation axis when the launch angle is different.

and the SD-E can adjust itself to the designed unique stable rolling state even if the axis deviates from the designed one due to external disturbances.

4.3. Enhancements of pipeline spanning detection via rolling stablization

Tests above have demonstrated that rotation is most stable when the SD is heavy enough and its mass is distributed on a plane. In order to demonstrate pipeline spanning detection enhancements after rolling stabilization, the lightest SD-A, the solid SD-D, and the disc-mounted SD-E were used to detect the vibration of a spanning pipeline. After the pipe was stimulate to vibrate, the excitation was stopped and the pipe continued freely vibrating with a resonance frequency of about 2.6 Hz. The performance of the SD of detecting spanning pipeline vibration is affected by two factors: frequency and amplitude of the pipeline vibration. In general, when the vibration frequency is greater than 5 Hz, the vibration can be reliably detected; when the vibration frequency is less than 5 Hz, it is difficult to distinguish the vibration frequency signal [23]. In terms of frequency alone, the lower the vibration frequency is, the more difficult the detection is. 2.6 Hz is a relatively low frequency, because the accelerometer is insensitive to low frequency vibration. The SD without structural optimization cannot stably roll around a fixed axis resulting a very low signal-to-noise ratio. In this case, it is difficult identify the pipeline vibration. The acceleration frequency spectrums obtained by the SD-A, SD-D, SD-E respectively inside a vibrating pipeline are shown in Figs. 14–16.

It can be seen that both the spectrums obtained by the SD-A and SD-D have only one peak that is the rolling frequency f_1, and have no peak related to the vibration frequency f_2; The rotation axes of the SD-A and the SD-D is none of the three sensitive axes of the accelerometer, since all the three components have one peak at the rotation frequency. In sharp contrast to this, the spectrum obtained by the SD-E has three peaks, $|f_1 - f_2|$, f_1, $f_1 + f_2$, because of stable axis-fixed rotation. The rotation axis of the SD-E is the Y axis of the accelerometer, since the Y component has no peak at the rotation frequency. This test demonstrates that low-frequency vibration of a pipeline can be easily detected by the opti-

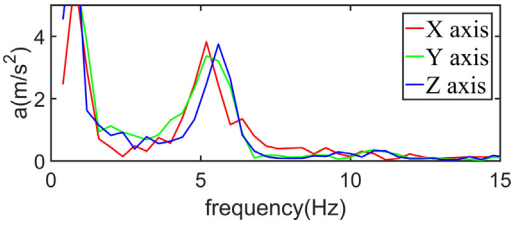

Fig. 14. Acceleration frequency spectrum obtained by the lightest SD-A inside a vibrating pipeline.

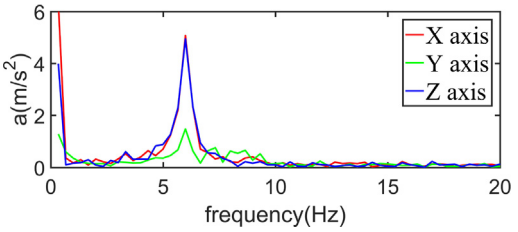

Fig. 15. Acceleration frequency spectrum obtained by the solid SD-D inside a vibrating pipeline.

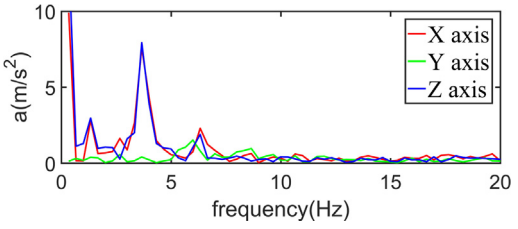

Fig. 16. Acceleration frequency spectrum obtained by the SD-E containing a steel disc inside a vibrating pipeline.

mized, fixed-axis-rotating SD. These characteristics of the spectrum obtained by the SD-E are consistent with Eqs.. (11)–(13).

As the SD can stably roll after structural optimization, the acceleration component in the direction of the rotation axis is always quite small; theoretically, it should be zero plus white noises. Therefore, this component can be used to distinguish the unstable state of the SD due to the external disturbance from the pipeline and the flow. According to the accelerometer output Eqs. (13)–(15), the other two components are equivalent to each other because they are both on the same plane perpendicular to the rotation axis, and their DC subcomponent is the centripetal acceleration and is proportional to the square of the rolling frequency.

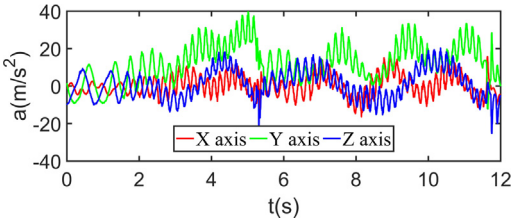

Fig. 17. Acceleration recorded by the lightest SD-A inside a bending down pipeline.

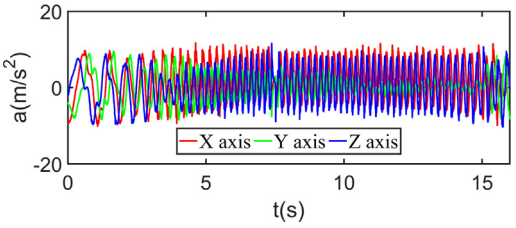

Fig. 18. Acceleration recorded by the solid SD-D inside a bending down pipeline.

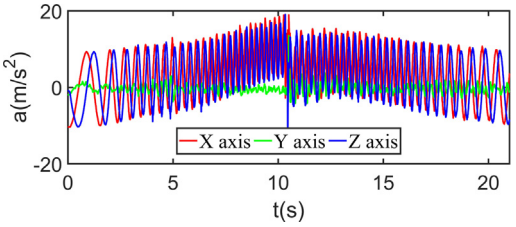

Fig. 19. Acceleration recorded by the SD-E containing a steel disc inside a bending down pipeline.

When the rolling speed of the SD changes, the DC subcomponent will significantly change as a consequence. Therefore, the stable-rolling SD can be used to detect a spanning and bent down pipeline.

For example, when the SD passes through one certain section of long span pipeline that has bent down, the SD will experience the process of downhill acceleration and uphill deceleration in sequence. As the rolling frequency becomes first larger and then smaller, the DC component will accordingly first increase and then decrease. However, this phenomenon only occurs when the SD is stably rotating. In order to demonstrate the decisive role of rolling stabilization in pipeline bend detection, the lightest SD-A, the solid SD-D, and the disc-mounted SD-E were used to roll inside a downward bent spanning pipeline. The results are shown in Figs. 17–19.

During the first two seconds, the SDs are speeding up in the PVC buffer pipe; after that, the SDs are passing through the spanning pipe that has bent down due to its own weight. The rotation axis of the lightest SD is significantly varying, and the acceleration/deceleration process cannot be seen at all. The solid SD can rolls more stably than the lightest SD, but its rotation axis is still changing as can be inferred from the amplitude fluctuation of the Y component; The rolling frequency gradually increases when the SD is climbing, but the decrease of the rolling frequency is not so noticeable when the SD is going downhill. As for the most stable SD-E, its rotation axis is always along the Y sensitive axis. The baseline of the recorded acceleration is noticeably going up first and then down in addition to the noticeable increase/decrease of the rolling frequency. In the middle of the pipe, the SD bounces, but in a moment it resumes the fixed axis rotation as before. Performance comparisons among the SDs with without structural optimizations are listed in Table 3 and some of the SDs are identical to those of previous published works.

4.4. Further discussions and suggestions

The operational and environmental loads may have effects on the resonance frequency of a spanning pipeline, but have no effect on the vibration detection performance of the SD. For example, the free vibration frequency of the pipeline used in the current experiment is about 2.6 Hz; When this pipeline is filled with oil and immersed in water, its resonance frequency may be shifted to other values, such as 2 Hz. Both 2.6 Hz and 2 Hz vibrations can be detected by the structure optimized SD. In other words, 2.6 Hz free vibration of the pipeline in air is equivalent to 3 Hz (for instance) resonance vibration of the same pipeline filled with oil and immersed in water. Therefore, the test results of the free

Table 3
Comparison of different SDs.

SD number	SD-A [20]	SD-B/SD-C	SD-D [23]	SD-E
Structure type	General structure without optimization	Having most of the mass concentrated in the cylindric core	Solid structure without optimization	Having most of the mass concentrated on the middle plane
Advantages	None	Simple internal structure and easy to implement	Very heavy and high-frequency noise is very small	Existence of a unique rotation axis with maximum moment of inertia
Shortcomings	Too light and is easy to be disturbed	Axis with maximum moment of inertia is not unique	Same moment of inertia in all directions and axis of rotation is arbitrary	None
Rolling state	Very unstable	Rolling axis is not unique and has risk of sudden change.	Rolling axis is always changing and acceleration amplitude continuously fluctuates.	Rolling axis is unique and the SD can recover to the axis-fixed rolling from a sudden disturbance.
Detectivity of low frequency vibration	Undetectable	Undetectable	Undetectable	Detectable
Detectivity of curved spanning pipeline	No noticeable feature	No noticeable feature	No noticeable feature	Noticeable features

vibration of the pipeline in this paper can ensure the validity of the SD for a field subsea spanning pipeline.

One should be cautious to put the SD into a field pipeline, especially a subsea pipeline. Once a detection accident occurs, the loss is very serious. Many tests of the SD have been carried out on field pipelines, including a pipeline in the mountainous area in Kunming, who has more than 10 m riser visible to the naked eye, as well as dozens of meters of climbing section in the mountain area. We have also tested the SD in the water supply pipeline with very large diameter (more than 800 mm), during which there was also no loss of the SD. These field experiments have demonstrated that the spherical detector can safely pass through a field pipeline and accomplish the detection task.

Many field experiences prompt us to summarize some main points to make sure the SD can be safely deployed and can collect high quality data. The pipeline should be unidirectional and has no branches, otherwise the SD may get lost. Before the SD is launched into the pipeline, pigging should be carried out first to ensure that the SD will not be blocked due to wax sediment and geometric deformation of the pipeline. The structure of the SD should be optimized for posture stabilization to enhance the performances of pipeline span inspection. The SD is very flexible and convenient to use and has many advantages in trafficability, but the pipeline has diversity, including the pipeline itself and the environment where the pipeline is located. It is suggested that scientists should do targeted research in combination with the specific state of the local pipeline while studying the SD.

5. Conclusion

This paper studies the decisive factors and stabilization methods of making the SD stably roll inside a pipeline, and experimentally demonstrates the feasibility and significance of rolling stabilization in pipeline spanning detection. Three main points can be concluded.

(1) The larger the weight of the SD is, the less likely the rolling state is to be disturbed. One of the ways to increase the stability of the SD is to properly increase the weight of the SD.
(2) If the mass of the SD is concentrated on a plane in the middle, the SD can stably roll around the unique fixed rotation axis perpendicular to that plane. Even if the rolling of the SD with this structure is disturbed, the SD can recover its previous rolling state quickly. Among several structures, it is the most stable and has most advantages.
(3) When the SD rotates around a fixed rotation axis, one sensitive axis of the triaxial accelerometer can be overlapped with the rotation axis through manual installation, and the effective information related to spanning pipeline bend and vibration will be transmitted to the other two sensitive axes with the highest signal-to-noise ratio. This type of SD can sensitively and reliably detect the low frequency vibration and down bend of the spanning pipeline.

CRediT authorship contribution statement

Guo Lin: Methodology, Writing - original draft, Investigation. **Zeng Zhoumo:** Funding acquisition, Project administration. **Huang Xinjing:** Methodology, Funding acquisition, Writing - review & editing, Project administration. **Li Mingze:** Investigation. **Feng Hao:** Conceptualization, Resources, Project administration. **Li Jian:** Funding acquisition, Project administration. **Rui Xiaobo:** Investigation.

Declaration of Competing Interest

The authors declare that they have no known competing financial interests or personal relationships that could have appeared to influence the work reported in this paper.

Acknowledgments

This work is supported by National Key Research and Development Project of China (No. 2016YFC0802103), National Natural Science Foundation of China (Nos 61773283, 51604192) and Project funded by China Postdoctoral Science Foundation (No. 2018M630271).

References

[1] P. Davis, J. Brockhurst, Subsea pipeline infrastructure monitoring: A framework for technology review and selection, Ocean Eng. 104 (Aug.) (2015) 540–548.
[2] A. Zakeri, Review of state-of-the-art: Drag forces on submarine pipelines and piles caused by landslide or debris flow impact, J. Offshore Mech. Arct. 131 (1) (2009) 403–410.
[3] J. Cai, X. Jiang, G. Lodewijks, Residual ultimate strength of offshore metallic pipelines with structural damage—A literature review, Ships Offshore Struc. 12 (8) (2017) 1037–1055.
[4] L. Cheng, K. Yeow, Z. Zang, F. Li, 3D scour below pipelines under waves and combined waves and currents, Coast. Eng. 83 (Jan.) (2014) 137–149.
[5] J.Y. Lee, J. Mcinerney, R. Cossu, et al., Predicting scour beneath subsea pipelines from existing small free span depths under steady currents, J. Ocean Eng. Sci. 2 (2) (2017) 61–75.
[6] M.M. Shabani, A. Taheri, M. Daghigh, Reliability assessment of free spanning subsea pipeline, Thin. Wall. Struct. 120 (2017) 116–123.
[7] T. Li, C. An, W. Liang, M. Duan, S.F. Estefen, Semi-analytical solution for soil-constrained vibration of subsea free-spanning pipelines, Ships Offshore Struc. 13 (6) (2018) 666–676.
[8] M. Mandal, P. Roy. Influence of pipeline specifications and support conditions on natural frequency of free spanning subsea pipelines, Adv. Struct. Eng. 1 (Jan.) (2015) 663–672.
[9] O. Ola, ROV based survey: A new, more effective approach, OTC. 4 (2016) 3070–3081.
[10] V.H. Fernandes, A.A. Neto, D.D. Rodrigues, Pipeline inspection with AUV, acoustics in underwater geosciences symposium, RIO Acoustics. (2015) 1–5.
[11] X.Y. Nie, Y.C. Yang, et al., Long-term monitoring system of submarine pipeline vibration based on fiber grating sensor technology, Proc. Int. Offshore Polar Eng. Conf. (2018) 230–237.
[12] M. Damien, G. Renaud, J. Yves, L. Vincent, Dynamic optical fiber sensing with brillouin optical time domain reflectometry: application to pipeline vibration monitoring, J. Lightwave Technol. 35 (16) (2017) 3296–3302.
[13] X. Zhao, L. Li, Q. Ba, et al., Scour monitoring system of subsea pipeline using distributed Brillouin optical sensors based on active thermometry, Opt. Laser Technol. 44 (7) (2012) 2125–2129.
[14] Wu Ruijuan, Zhu Baikang, Tu Qinchang, Application of Optical Fiber Sensing Technology in Operation Monitoring of Submarine Pipeline, China Water Transport. 17 (5) (2017) 303–306. (In Chinese)
[15] J. Quarini, S. Shire, A review of fluid-driven pipeline pigs and their applications, Proc. Inst. Mech. Eng. E, J. Process Mech. Eng. 221 (1) (2007) 1–10.
[16] H.S. Han, J.J. Yu, C.G. Park, J.G. Lee, Development of inspection gauge system for gas pipeline, KSME Int. J. 18 (3) (2004) 370–378.
[17] F. Richard, C. Muthu, SmartBall: A new approach in pipeline leak detection, 2008 ASME International Pipeline Conference 2 (2008) 117–133.
[18] S.X. Guo, S.L. Chen, X.J. Huang, T.S. Xu, Design of a spherical leak detector for submarine oil pipelines, Appl. Mech. Mater. 709 (Dec.) (2015) 460–464.
[19] S. Guo, S. Chen, X. Huang, Y. Zhang, S. Jin, CFD and experimental investigations of drag force on spherical leak detector in pipe flows at high Reynolds number, Cmes-comp. Model. Eng. 101 (1) (2014) 59–80.
[20] X. Huang, S. Chen, S. Guo, X.u. Tianshu, Q. Ma, S. Jin, G.S. Chirikjian, A 3D localization approach for subsea pipelines using a spherical detector, IEEE Sens. J. 17 (6) (2017) 1828–1836.
[21] H. Xinjing, C. Guanren, Y.u. Zhang, X.u. Li Jian, C.S. Tianshu, Inversion of magnetic fields inside pipelines: modeling, validations, and applications, Struct. Health. Monit. 17 (1) (2018) 80–90.
[22] Zhang Yu, X. Yameng, H. Xinjing, Jian Li, C. Shili, Pipeline inclination measurements based on a spherical detector with magnetic proximity switches, IEEE Access. 6 (2018) 39936–39943.
[23] G. Lin, Z. Zhoumo, H. Xinjing, L.i. Jian, C. Shili, Vibration detection of spanning subsea pipelines by using a spherical detector, IEEE Access. 7 (2019) 7001–7010.